

Surface oxidation of hydrophobic ZnSe for enhanced growth of atomic layer deposited aluminum oxide

Corbin Feit¹, Jaynlynn Sosa², Alexandros Kostogiannes³, Matthieu Chazot³, Nicholas G. Rudawski⁴, Titel Jurca^{2,5,6}, Kathleen A. Richardson^{1,3}, Parag Banerjee^{1,2,6,7}*

¹Department of Materials Science and Engineering, University of Central Florida, Orlando, FL 32816

²NanoScience and Technology Center (NSTC), University of Central Florida, Orlando, FL 32816

³CREOL, College of Optics and Photonics, University of Central Florida, Orlando, FL 32816, USA

⁴Research Service Centers, University of Florida, Gainesville, FL 32611, USA

⁵Department of Chemistry, University of Central Florida, 4111 Libra Drive, Orlando, FL 32816, USA

⁶Renewable Energy and Chemical Transformation (REACT), Faculty Cluster Initiative, University of Central Florida, Orlando, FL 32816

⁷Florida Solar Energy Center, University of Central Florida, Orlando, FL 32816

AUTHOR INFORMATION

Corresponding Author

*Parag Banerjee, Department of Materials Science and Engineering, University of Central Florida, Orlando, FL – 32816, USA, parag.banerjee@ucf.edu .

ABSTRACT

The growth of atomic layer deposited (ALD) Al₂O₃ on planar ZnSe substrates is studied using *in situ* spectroscopic ellipsometry. An untreated ZnSe surface requires an incubation period of 27 cycles of ALD Al₂O₃ before film growth is observed. Pretreating the surface with ultraviolet generated ozone lowers the incubation to 17 cycles, whereas a plasma enhanced ALD Al₂O₃ process can further lower the incubation period to 13 cycles. The use of ozone or plasma-activated oxygen species on ZnSe is found to create ZnO and SeO₂ which are responsible for converting the ZnSe from a hydrophobic to a hydrophilic surface. The interfacial layer between Al₂O₃ and ZnSe is mapped using high-resolution transmission electron microscopy and scanning transmission electron microscopy / energy dispersive spectroscopy. The SeO₂ is volatile and leaves a zinc-rich interface which is 4.3 nm thick for the ultraviolet generated ozone pretreated sample and 2.5 nm for the plasma enhanced ALD process.

KEYWORDS Atomic layer deposition, aluminum oxide, zinc selenide, UV-ozone treatment.

I. Introduction

ZnSe is a II–VI wide bandgap semiconductor with a direct band gap¹ of 2.67 eV and an exciton binding energy of 20 meV.² It is intrinsically *n*-type with a doping density of 10^{15} cm⁻³ and can be extrinsically doped *n*-type using Al or Cl or, *p*-type using nitrogen plasma.^{3,4} ZnSe also offers low absorption in the IR spectral region, can be scalably manufactured and is mechanically robust.^{5,6} These properties make ZnSe a versatile material in bulk, thin film or fiber form for active and passive use in optoelectronic devices such as, UV photodetectors,³ light emitting diodes⁷, laser diodes⁸, lenses, IR transparent windows and optical fibers.³⁻¹⁰

Development of ZnSe-based optoelectronic devices depends on the ability to control ZnSe surfaces and interfaces. For example, devices such as photodetectors and laser emitting diodes require high-quality epitaxially matched ZnSe thin films on GaAs substrates.⁹⁻¹¹ Recent efforts to dope ZnSe crystals with transition metals such as Cr²⁺ or Fe²⁺, have yielded active single crystal laser host materials, which emit in the spectrally important mid-infrared (MIR) region.¹² In contrast to ZnSe thin films, recent developments in mid-IR optical fiber laser systems have explored the potential to capture the desirable attributes of difficult to grow single crystals of Fe or Cr-doped ZnSe in host matrices; hence here, the use of optically active ZnSe particles embedded in a parent glass matrix results in the formation of a highly functional, complex optical composite.¹³⁻¹⁸ The synthesis for such composites impart stringent requirements on the stability of the ZnSe particle in the parent matrix during high temperature melting, fabrication and drawing processes of fibers. Here, any degradation of the dopant crystal, or processing protocols that impart undesirable impurities into the matrix that hinders the absorption or emission behavior of the active species, are to be avoided.¹⁹ To this end, the possibility of using the robust conformal nature of

atomic layer deposition to passivate the dopants surface to enhance its stability in a composite, is highly desirable.

The varied requirements for ZnSe-based optoelectronic devices creates the need to understand conditions that lead to favorable growth of materials on ZnSe surfaces. While many techniques exist to deposit films on planar substrates, atomic layer deposition (ALD) provides the only avenue to deposit functional films with monolayer fidelity on planar and powder substrates, alike. Previously, ZnSe crystalline substrates have been used as transmission medium to study *in situ* infrared spectroscopy of Al₂O₃ ALD.²⁰ However, little is known about initiating ALD reactions on the surface of ZnSe itself. This study evaluates the fundamental mechanism of Al₂O₃ ALD growth on planar ZnSe.

We present a surface chemistry approach to understand the nature of ALD film growth on ZnSe surface. On a planar ZnSe substrate, an Al₂O₃ layer may represent a gate dielectric layer used in a transistor, while a conformal Al₂O₃ on a ZnSe particle may provide protection against dissolution during high temperature synthesis of mid-IR optical materials.²¹ The underpinning of these varied requirements requires first, the manipulation and control of the surface chemistry of ZnSe. It is shown that a pre-deposition oxidation step or the use of O₂ plasma as a co-reactant can change the surface chemistry of ZnSe from hydrophobic to hydrophilic due to the formation of SeO₂. The formation of a selenium oxide layer leads to shorter incubation cycles and growth of ALD Al₂O₃ on a planar substrate.

II. Experimental Details

A Fiji Gen2 PEALD system from Veeco® with an Ebara® multi-stage dry vacuum pump A30W (pumping speed 3600 liters/minute) was used to deposit Al₂O₃ films on ZnSe wafers. The base

pressure of the ALD chamber was maintained at 5×10^{-7} Torr with a working pressure of ~ 120 mTorr. The ALD process consisted of alternating pulses of trimethylaluminum (TMA) (Millipore Sigma) = 0.06 seconds and deionized water (DIW) pulse = 0.06 seconds, each separated with an Ar purge for 15 seconds. The purge is longer than necessary as it allows for recording of the *in situ* data via ellipsometry with sufficient frequency and fidelity. The deposition of Al_2O_3 was conducted at 175°C . As an alternate, a PEALD Al_2O_3 process at 175°C consisting of 0.06 seconds of TMA and O_2 plasma (300 W for 4 seconds) was used as well.

The deposition rate of the film was monitored by *in situ* spectroscopic ellipsometry using a J. A. Woollam[®] M-2000, with a wavelength range from 273 to 1690 nm. The thickness was modeled using the COMPLETE EASE[®] software, consisting of a Cauchy layer optimized with Al_2O_3 optical constants on a ZnSe substrate layer (ZnSe model provided in the CompleteEASE[®] substrate library).

The ZnSe substrate (10 mm in diameter) were supplied by EKSMA Optics USA DBA Altos Photonics, Inc. A piece of black carbon paper was placed under the ZnSe substrate to prevent any backside reflection from the ZnSe (see **Figure 1**, inset). The ZnSe substrates were ultrasonically cleaned with isopropyl alcohol (IPA) and DIW. For the case where surface oxidation of ZnSe was required, a 15-minute exposure to UV- O_3 was conducted on a Model E511 made by Ossila[®]. The dominant wavelengths of the UV light are 185 nm and 254 nm. The lamp power is $20 \mu\text{W}/\text{cm}^2$. To optically model this substrate, a Cauchy layer (i.e., insulator) was used on a ZnSe substrate. The resulting model consistently predicted a ~ 4 nm film, identified as SeO_2 using XPS. This interfacial layer was kept fixed during the modeling of the subsequent ALD Al_2O_3 . Prior to ALD, static water contact angle (WCA) measurements were taken on an Ossila[®] E511 and analyzed

using Ossila® contact angle software (Version 1.1.02). DIW droplets of a volume of 10 μ L were dropped using pipette on untreated and UV-O₃ treated ZnSe film substrates.

The changes to the ZnSe surface chemistry were probed by x-ray photoelectron spectroscopy (XPS) using an ESCALAB-250Xi XPS system from ThermoFisher Scientific®. Experiments were performed at a pressure below 7 x 10⁻⁹ mbar using Al-K α monochromatic radiation and operating power of 300 W (15 kV, 20 mA). XPS data analysis and peak deconvolutions were analyzed using the open source XPS Peak 41 software. Binding energies were calibrated using C 1s peak at 284.5 eV.

An FEI® Themis Z scanning/transmission electron microscopy (S/TEM) with Cs probe correction was used to analyze the Al₂O₃/ZnSe interfaces; the operating voltage was 200 kV and the system is equipped with a monochromator, a bottom-mounted FEI Ceta 16M CMOS camera, a Fischione Instruments Model 3000 high angle annular dark-field (HAADF) STEM detector, and a SuperX windowless SDD energy dispersive spectroscopy (EDS) system (solid angle of collection = 0.67 sr). Conventional high-resolution (HR-TEM) imaging, HAADF-STEM imaging, and STEM-EDS mapping were performed; for HAADF-STEM work, the probe semi-angle of convergence was 22 mrad and the probe current was set to ~20 pA for high-resolution imaging and ~400 pA for STEM-EDS mapping; the inner collection angle of the HAADF detector for HAADF-STEM imaging was ~70 mrad. An *in situ* lift-out method using an FEI Helios Nanolab 600i dual focused ion beam/scanning electron microscope was used to extract and prepare lamellas for S/TEM analysis from the specimens as described elsewhere,²²⁻²⁴ prior to preparation of the lamellas, the specimens were ex situ coated with ~50 nm of Cr using electron beam evaporation to protect/preserve the Al₂O₃ film and film/substrate interface.²⁵

Image J® was used for analysis of TEM images. Thickness measurements were made on cross-section images. A set of 20 measurements were usually made to obtain statistically rigorous averages and standard deviations obtained.

III. Results and Discussion

The growth behavior of 100 cycles of ALD Al_2O_3 is captured via *in situ* ellipsometry in **Figure 1** for three planar samples: 1) untreated ZnSe, 2) ZnSe treated with 15 minutes of ultraviolet – ozone (UV- O_3), and 3) untreated ZnSe with a plasma-enhanced ALD (PEALD) Al_2O_3 process with O_2 plasma as an oxidant. The Al_2O_3 thickness variation is plotted as a function of deposition

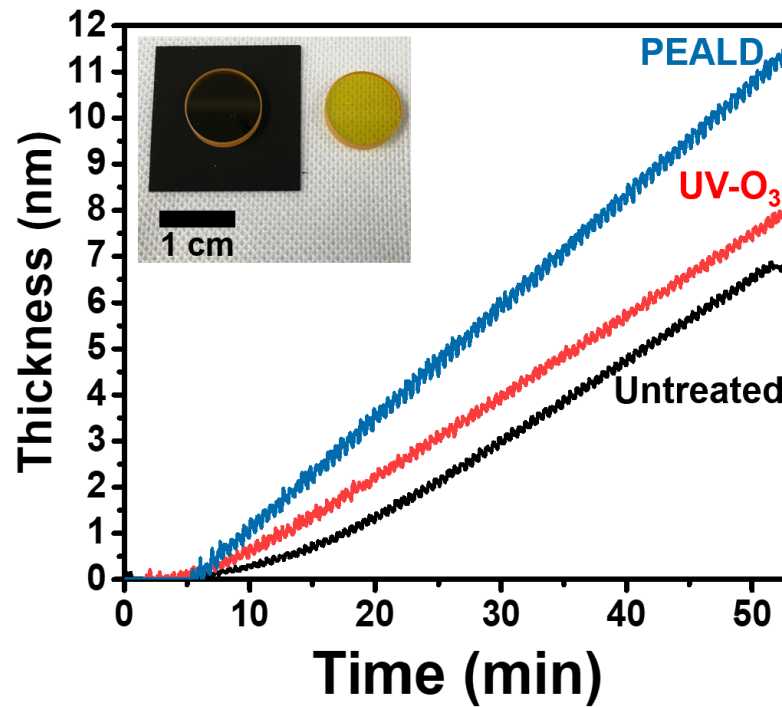


Figure 1. *In situ* growth curves obtained via spectroscopic ellipsometry for 100 cycles of ALD Al_2O_3 deposited at 175 °C on ZnSe substrates. The untreated ZnSe shows the longest incubation period and results in a final Al_2O_3 thickness of 6.7 nm. The UV- O_3 pretreated ZnSe results in Al_2O_3 thickness of 7.8 nm. The PEALD process yields the shortest incubation and results in a final Al_2O_3 thickness of 11.3 nm. Inset: ZnSe coupons are transparent (right) and must be kept on carbon paper (left) to prevent backside reflection during *in situ* ellipsometry measurements.

	Thickness via ellipsometry (nm)	Interfacial thickness via ellipsometry (nm)	Thickness via TEM (nm)	Interfacial thickness via TEM (nm)	Incubation period (cy)	Steady state growth rate (nm/cy)
Untreated	6.8 ± 0.026	-	5.9 ± 1.4	-	27	0.093
UV-O ₃	7.8 ± 0.029	4.0	7.1 ± 1.2	4.3 ± 0.6	17	0.094
PEALD	11.3 ± 0.026	-	11.2 ± 0.6	2.5 ± 0.3	13	0.130

Table 1. ALD growth parameters of Al₂O₃ extracted from *in situ* spectroscopic ellipsometry on untreated ZnSe (1st row) and ZnSe treated with 15 minutes of UV-O₃ prior to deposition (2nd row). Both the samples were subjected to thermal ALD using TMA and H₂O. The 3rd row shows PEALD of Al₂O₃ using TMA and O₂ plasma on untreated ZnSe. The temperature of deposition was maintained at 175 °C across all three samples. Additionally, the thickness measurements from cross-section TEM are listed and show good correlation with ellipsometry.

time (in minutes). The untreated ZnSe exhibits the longest incubation period of 27 ALD cycles until linear growth rate (0.093 nm/cy) of Al₂O₃ is achieved. Here the incubation cycle, c is calculated as $c = 100 - \frac{t}{g}$, where t = final thickness (nm) at 100 cycles, and g = growth rate (nm/cy). The delay in nucleation results in the thinnest Al₂O₃ film of 6.8 nm after 100 cycles. On the other hand, pretreating with UV-O₃ alters the surface chemistry of ZnSe and shortens the incubation delay of Al₂O₃ to 17 cycles. As a result, a 7.8 nm Al₂O₃ film is obtained after 100 ALD cycles with a steady state growth rate in the linear regime of 0.094 nm/cy. Finally, the PEALD process shows the shortest incubation period of 13 cycles on an untreated ZnSe surface. The growth at the end of 100 cycles is 11.3 nm and the steady-state growth rate in the linear regime is 0.130 nm/cycle, which is in good agreement with an O₂ plasma ALD of Al₂O₃ on a ZnSe and silicon substrates.^{20, 26} These data are collectively summarized in **Table 1**. The data suggests that a pretreatment of ZnSe surface with UV-O₃ or, use of a strong oxidant such as an O₂ plasma during ALD reduces the incubation delays and improves growth characteristics of Al₂O₃ on ZnSe surface.

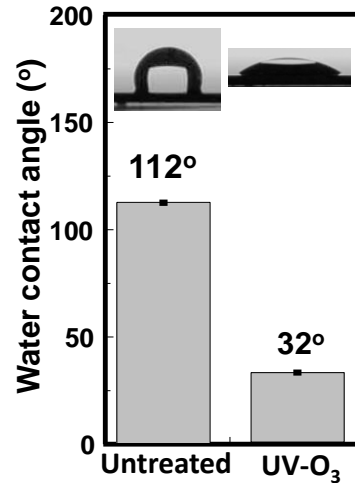


Figure 2. Static water contact angle measurements on untreated ZnSe and UV-O₃ ZnSe substrates. The untreated sample is hydrophobic (contact angle ~112°) whereas exposing to UV-O₃ converts the substrate surface to hydrophilic (contact angle ~32°).

Additionally, final film thickness is also determined via HRTEM of film cross-sections and is presented in **Table 1**. Good correlation is observed between ellipsometry and TEM. The TEM results are discussed in greater detail below.

Static water contact angle (WCA) measurements were performed to understand the surface chemistry of ZnSe planar substrates and the effect of surface oxidation (**Figure 2**). The untreated ZnSe surface is hydrophobic with a contact angle of 112° which is consistent with previous reports for bulk ZnSe.²⁷ Upon UV-O₃ treatment, the WCA reduces to 32° indicating the hydrophilic nature of the oxidized surface. The WCA results from planar substrates helps to infer that the UV-O₃ treatment can improve the wettability of ZnSe, resulting in enhanced nucleation and growth of Al₂O₃ ALD. This result indicates that if functional ALD coatings are required on ZnSe, surface oxidation is necessary to enhance coating adherence and conformal coverage. While other modifications may lead to similar

results, surface oxidation through UV-O₃ or oxygen plasma are straightforward processes that result in enhanced nucleation and growth on ZnSe.

In order to confirm the oxidation state of the ZnSe surface after pretreatment, the ZnSe substrates were probed by XPS. The Zn 2p spectra of the as-received Zn-Se is shown in **Figure 3(a)**. The

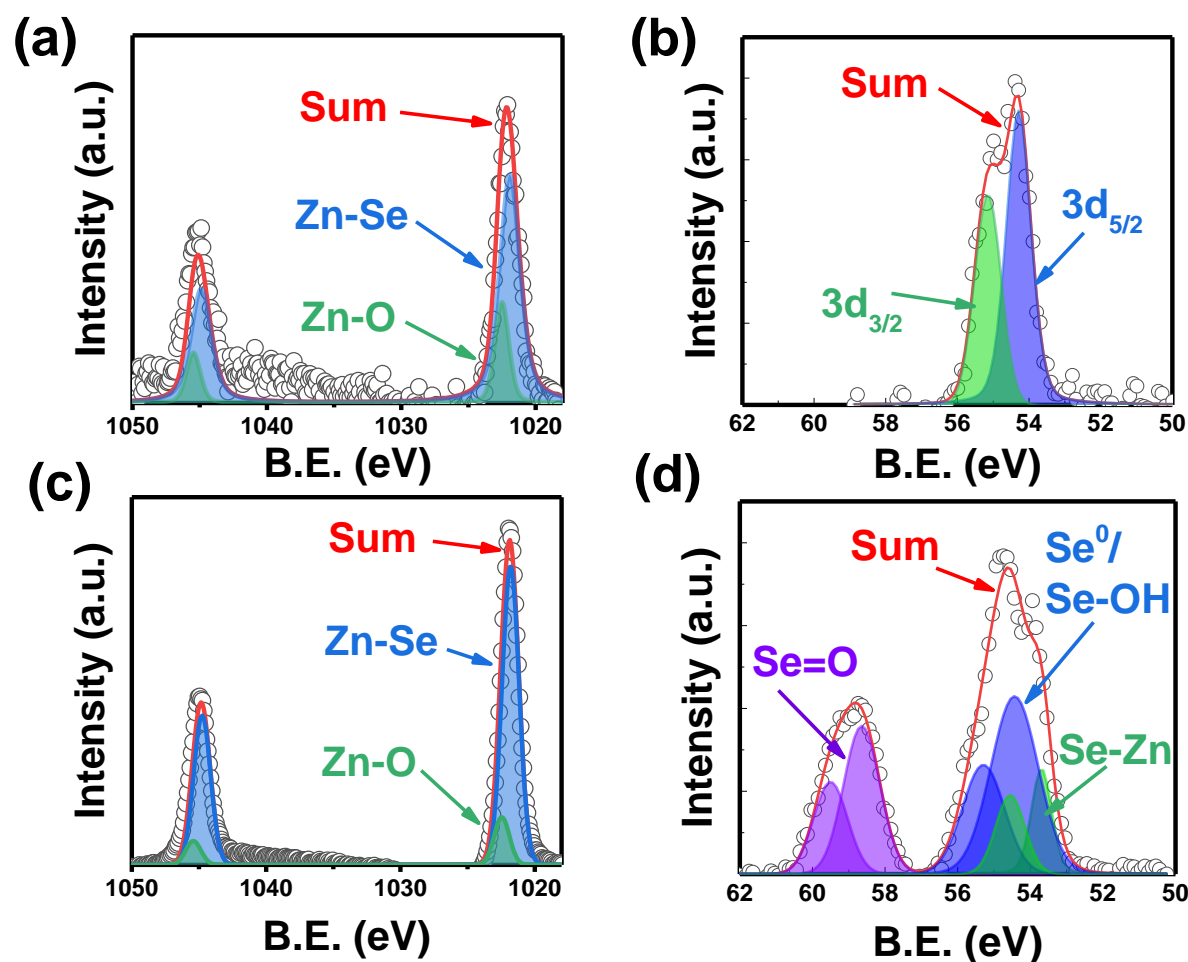


Figure 3. (a) XPS high-resolution spectrum of Zn 2p from the untreated, as-received ZnSe showing primarily Zn-Se bonding with a little Zn-O bonding. (b) XPS high-resolution spectrum of Se 3d from untreated, as-received ZnSe showing Se-Zn bonding. (c) XPS high-resolution spectrum of Zn 2p from the UV-O₃ treated ZnSe showing primarily Zn-Se bonding with a little Zn-O bonding, similar to the untreated ZnSe sample. (d) XPS high-resolution spectrum of Se 3d from the UV-O₃ treated ZnSe showing Se-Zn bonding but importantly, Se-O formation as well. All peaks were normalized

spectrum can be deconvoluted into two peaks. The Zn 2p_{3/2} binding energy (B.E.) peak at 1021.98 eV corresponds to the Zn-Se bonding, whereas the peak at 1022.57 eV corresponds to Zn-O.^{28, 29} Even with ZnO detected via XPS, the surface properties of ZnSe remain hydrophobic suggesting limited oxidation of the surface. In **Figure 3(b)**, the Se 3d high-resolution spectrum shows peaks at 54.15 eV and 55.01 eV corresponding to Se 3d_{5/2} and Se 3d_{3/2}, respectively. These peaks are related to the Se-Zn bond. We note that the peaks are closely separated with a spin-orbit splitting of 0.86 eV only.³⁰

The Zn high-resolution spectra of the ZnSe substrate pretreated with UV-O₃ is shown in **Figure 3(c)**. Similar to the untreated ZnSe surface, the Zn 2p_{3/2} peak are present at higher B.E. - 1021.8 eV for Zn-Se and 1022.45 eV for Zn-O. Increased elemental ZnO or ZnOH after UV-O₃ treatment is observed.²⁹ The effect of UV-O₃ pretreatment on the Se is shown in **Figure 3(d)**. After UV-O₃ pretreatment, the primary B.E. of the Se 3d_{5/2} can be seen to split into two. The lower B.E. pair with Se 3d_{5/2} at 53.69 eV corresponds to ZnSe, whereas the higher B.E. Se 3d_{5/2} at 54.64 eV corresponds to elemental (Se⁰) or, can also be assigned to Se-OH^{29, 31}. Additionally, B.E. peaks are observed at 58.64 eV (3d_{5/2}) and 59.5 eV (3d_{3/2}) corresponding to the Se-O bond formation.^{28, 29, 31} The oxidation of the ZnSe is considered to cleave the Zn-Se bonding to form SeO₂.³² It is possible that elemental Se may exist at the surface, but the B.E. is convoluted with Se(OH)₄ species.²⁹ Thus, the XPS analysis reveals that pretreating ZnSe with UV-O₃ generates oxides of Se.^{27-29, 31, 32} While ZnO is present on the surface of untreated ZnSe as well, presence of SeO₂ is observed upon UV-O₃ pretreatment. In light of these findings, it can be concluded that the presence of Se oxide helps the conversion of ZnSe surface from hydrophobic to hydrophilic.

We next focus on the surface chemical state of the Al₂O₃ ALD on ZnSe. In **Figure 4(a)** and **Figure 4(b)**, the Al 2p and O 1s high-resolution spectra are shown for the 7.8 nm Al₂O₃ grown on

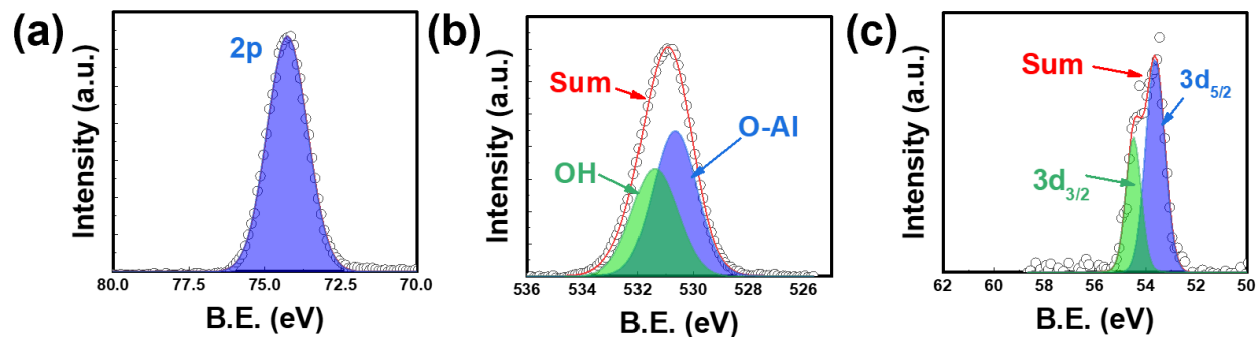


Figure 4. (a) Al 2p high-resolution spectra of 7.8 nm ALD Al₂O₃ on UV-O₃ treated ZnSe. (b) O 1s high-resolution spectra of the 7.8 nm ALD Al₂O₃ on UV-O₃ treated ZnSe. (c) Se 3d high-resolution spectra observed on the 7.8 nm ALD Al₂O₃ on UV-O₃ treated ZnSe. This was the only UV-O₃ pretreated ZnSe, respectively. The average escape depth of electrons from amorphous Al₂O₃ is ~ 3 nm,³³ and thus, it is unlikely that Zn or Se related to the ZnSe substrate can be detected. The Al 2p is centered at 74.26 eV whereas the O 1s can be deconvoluted into two species. The peak at 530.69 eV is attributed to the O bonding with Al whereas, the peak at 531.44 eV is associated with surface bound OH groups.³⁴ In this respect, the Al and O high-resolution spectra are unremarkable.

Surprisingly, in addition to Al and O signals, a signal from Se is also obtained. This is shown in **Figure 4(c)**. The Se 3d_{5/2} is positioned at 53.61 eV. This peak cannot be related to ZnSe, as no Zn was detected. The peak position is also not related to Se⁰ / Se-OH as shown previously in **Figure 3(d)**, as that peak lies at 54.64 eV *i.e.*, almost 1 eV higher. We speculate that the Se discovered on the ALD Al₂O₃ surface is likely bonded to Al as Al_xSe_y. A previous study by Chen *et al.*, report this behavior where, Al evaporated on ZnSe surfaces yields a Se core spectrum similar ZnSe.³⁵ The complimentary Al high-resolution spectra is unable to resolve the bonding as the Al-O and Al-Se peaks overlap.

Furthermore, it has been verified through XPS (not shown) of the ALD Al_2O_3 on untreated ZnSe (thinner, and at thickness 6.8 nm) and PEALD Al_2O_3 (thicker, and at thickness 11.3 nm) that Se signal is absent on these surfaces. While the partial diffusion of Se cannot be ruled out for the PEALD sample, it is likely that the origin of the Se detected on the UV- O_3 pretreated sample is due to the out-diffusion of Se from the $\text{Al}_2\text{O}_3/\text{ZnSe}$ interface.

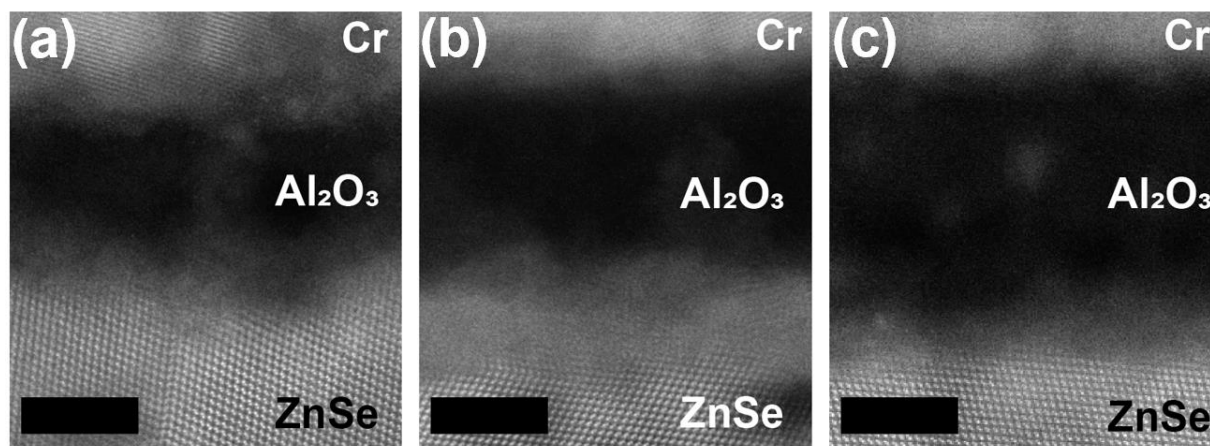


Figure 5. HAADF-STEM images of (a) untreated ZnSe coated with Al_2O_3 ALD. (b) UV- O_3 treated ZnSe coated with Al_2O_3 ALD and (c) untreated ZnSe coated with Al_2O_3 PE-ALD. Scale bar = 5 nm.

Both Se and SeO_2 are volatile species and known to sublime above $100\text{ }^\circ\text{C}$.³⁶⁻³⁸ The XPS data suggests that the Se in its elemental or, oxide form is mobile within the amorphous Al_2O_3 matrix. The detection of Se on the surface of Al_2O_3 for a UV- O_3 pretreated sample suggests that Se migration to the surface followed by volatilization may occur during the deposition process.

HAADF-STEM cross-section images are shown in **Figure 5** for all three samples. We note that the ZnSe is a polycrystalline substrate where a majority of the grains have an out-of-plane crystallographic orientation along $[110]$ direction. In **Figure 5(a)**, untreated ZnSe with amorphous Al_2O_3 coating is shown. The Al_2O_3 ALD film is measured to be 5.9 ± 1.4 nm. In **Figure 5(b)**, UV- O_3 pretreated ZnSe with Al_2O_3 coating is shown. An Al_2O_3 film of 7.1 ± 1.2 nm can be measured.

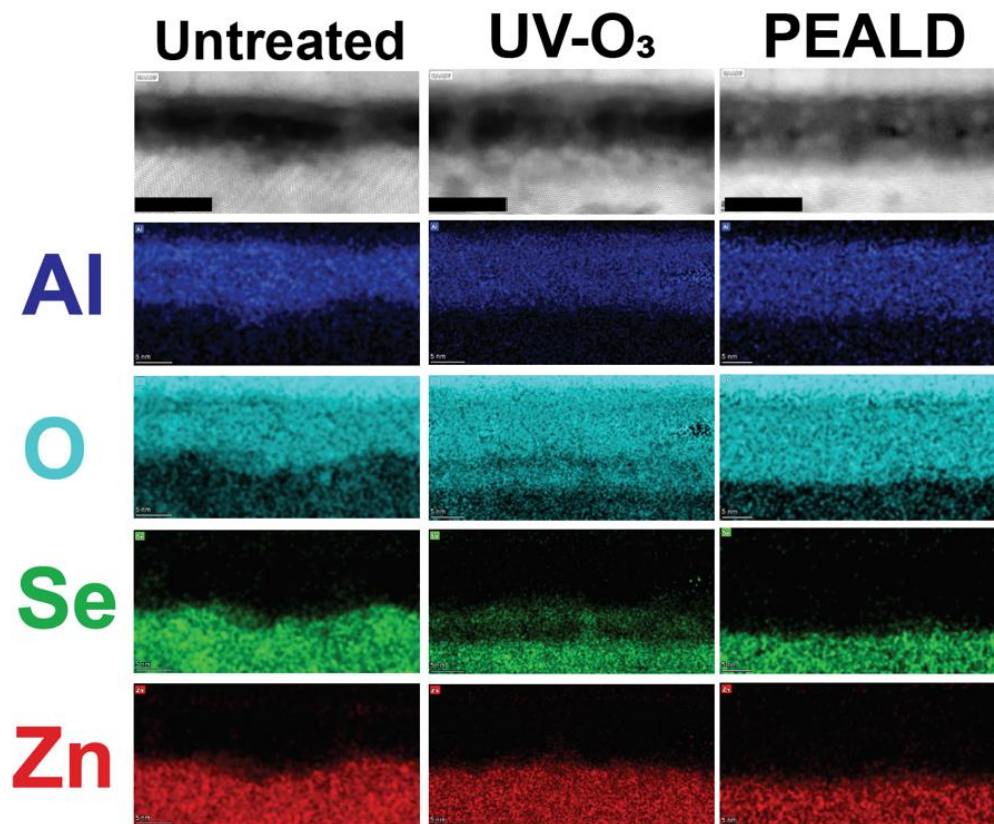


Figure 6. Elemental maps of untreated ZnSe coated with Al₂O₃ ALD (1st column); UV-O₃ treated ZnSe coated with Al₂O₃ ALD (2nd column) and, untreated ZnSe coated with Al₂O₃ PEALD (3rd column) indicating position of Al (blue), O (teal), Se (green) and Zn (red). Scale bar = 10 nm.

In addition, an interfacial region of approximately 4.3 ± 0.6 nm is measured corresponding to the SeO₂. The interfacial region appears amorphous, albeit lighter in contrast than Al₂O₃. This is consistent with ~ 4 nm SeO₂ film predicted by spectroscopic ellipsometry and confirmed by XPS. In **Figure 4C**, as-received ZnSe with Al₂O₃ PE-ALD coating is shown. An Al₂O₃ film of approximately 11.2 ± 0.6 nm can be measured. However, the thickness of the SeO₂ layer is 2.5 ± 0.3 nm due to the short exposure time of the ZnSe to O₂ plasma before the Al₂O₃ starts to conformally grow and protect the underlying ZnSe substrate. These results are presented collectively in **Table 1**, and show good correlation with *in situ* ellipsometry data.

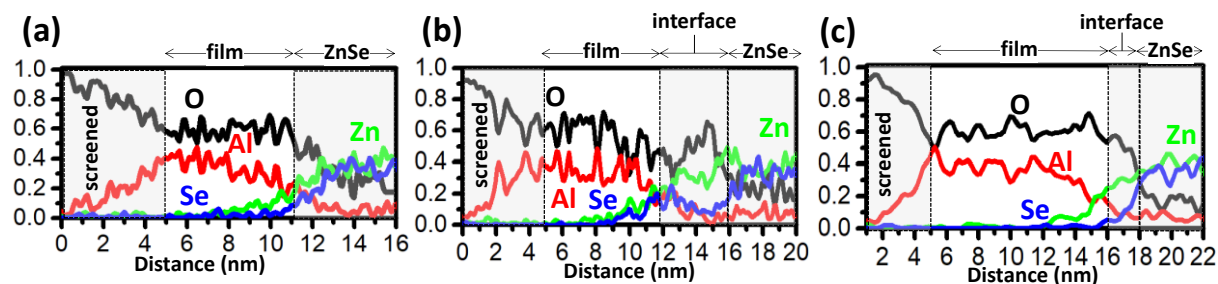


Figure 7: STEM-EDS line scans of (a) Untreated, (b) UV-O₃ pretreated and (c) PEALD Al₂O₃ films. The line scans correspond to normalized counts for O (black), Se (blue), Al (red) and Zn (green). The approximate location of the film and ZnSe substrate are shown on the top, x-axis, whereas the bottom x-axis is distance in nm.

STEM-EDS elemental mapping of the cross-sections of Al₂O₃ ALD on the three samples are shown in **Figure 6**. The Al is shown in blue, Zn in red, O in teal, and Se in green. The Al₂O₃ deposited on untreated ZnSe shows uniform distribution of Al and O with a sharp transition to the Zn and Se signals. The Zn and Se signals overlap indicating the presence of ZnSe. For the Al₂O₃ deposited on pretreated UV-O₃ sample, the O spread is much wider than the Al, extending partially into the substrate. This shows the presence of an O-rich interface layer, in line with the XPS and HAADF-TEM data. Further, the Se appears to extend upwards into the Al₂O₃ film, leaving behind a Se-depleted layer, while the Zn is rather uniform. Finally, the scan from the PEALD sample reveals the O signal extending deeper into the ZnSe than the Al. The Zn and Se signals overlap.

To quantify these observations further, the STEM-EDS elemental line scans are shown in **Figure 7(a), (b)** and **(c)** for the untreated, UV-O₃ and PEALD samples, respectively. The y-axis are the normalized intensity counts. To demarcate the various regions probed, the following procedure is adopted. The region next to origin on the x-axis, (i.e., distance = 0 nm) consists of the Cr layer which is deposited on top of the Al₂O₃ film during sample preparation. The O signal rises in this region due to formation of chromium oxide. Thus, to conduct the analysis at the Al₂O₃ film/ ZnSe

substrate interface, the data are screened first. The distance at which the O counts first decrease and then stabilize is noted to be the top interface between Cr and Al₂O₃. The analyses from this point onwards till the measured film thickness (determined via HAADF images) encompasses the Al₂O₃ layer and beyond that, the ZnSe substrate. As expected, the Zn:Se ratio in the substrate is nearly 1:1. These regions are demarcated on the top x-axis for all the three samples.

For the untreated sample shown in **Figure 7(a)**, Zn and Se decrease monotonically with the Zn extending slightly deeper into the Al₂O₃. The Zn signal extends 3 nm inside the oxide ($8 \text{ nm} \leq x \leq 11 \text{ nm}$). For the UV-O₃ treated sample shown in **Figure 7(b)**, the interface is different. The Zn and Se signals extend inside the film, while the interface ($12 \text{ nm} \leq x \leq 16 \text{ nm}$) appears to have a distinct layer that is Se depleted i.e., Zn rich. It is also noted that the O signal rises briefly in this region. For the PEALD sample shown in **Figure 7(c)**, the interface ($16 \text{ nm} \leq x \leq 18 \text{ nm}$) appears to be Zn-rich. The Zn region extends 4 nm inside the film ($12 \text{ nm} \leq x \leq 16 \text{ nm}$).

The trend for the Zn to extend deeper into the Al₂O₃ film compared to the Se can be explained by the high volatility of SeO₂. For the case of the untreated sample, the amount of Se lost depends on duration of the incubation cycles in which the H₂O is oxidizing the ZnSe surface, converting the Zn to ZnO and Se to SeO₂. The SeO₂ can be subsequently volatilized. Here we note that the SeO₂ has a room temperature vapor pressure of 2×10^{-6} Torr.³⁹ Since the deposition temperature for ALD is 175 °C and working pressure in the ALD chamber is 120×10^{-3} Torr, the SeO₂ vapor pressure is expected to be much higher than the room temperature reported value and comparable to the ALD working pressure. For the case of the UV-O₃ pretreated sample, there is significant SeO₂ formation on the surface *prior* to the start of the ALD process. This SeO₂ will volatilize leaving a Zn-rich, oxide region that is distinctly seen in **Figure 7(b)** for $12 \text{ nm} \leq x \leq 16 \text{ nm}$. Additionally, the Zn and Se signal between $8 \text{ nm} \leq x \leq 12 \text{ nm}$ attenuates in the same way as

shown in **Figure 7(a)** from $8 \text{ nm} \leq x \leq 11 \text{ nm}$, since the H_2O based ALD chemistry remains unchanged. Thus, we hypothesize the ALD process causes the Zn and trailing Se tails to be present in the oxide as evidence of the Al_2O_3 nucleation process. For the PEALD process the SeO_2 formation is more aggressive in the presence of the O_2 plasma. Thus, the loss of Se in **Figure 7(c)**, $16 \text{ nm} \leq x \leq 18 \text{ nm}$, is more severe. This leads to faster nucleation of the Al_2O_3 . The Al_2O_3 protective layer formed above limits subsequent oxidation of ZnSe. As a result, the interface is only 2 nm thick.

IV. Conclusions

In conclusion, we have demonstrated that ALD Al_2O_3 on ZnSe depends on the state and degree of oxidation of the ZnSe surface. An untreated ZnSe substrate requires an incubation of 27 cycles before ALD Al_2O_3 can be grown on the surface. Pretreating the ZnSe substrate with a UV- O_3 exposure reduces the incubation to 17 ALD cycles, while switching to a PEALD process lowers the incubation period to 13 ALD cycles. Extensive characterization of the ZnSe surface and Al_2O_3 / ZnSe interface reveals oxidation of the Zn, but more importantly, Se upon UV- O_3 pretreatment. This interface layer is measured to be $\sim 4.3 \text{ nm}$ in width. Further, the Se in the UV- O_3 pretreated sample appears to be highly diffusive in nature and migrates to the top of the Al_2O_3 surface. On other hand, the PEALD process results in a thinner interface of $\sim 2.5 \text{ nm}$. In both cases, the interface is left Zn-rich in nature, revealing the volatile nature of the Se, when oxidized. These findings will aid in the understanding of developing reliable and robust coatings on ZnSe substrates for optoelectronics devices.

V. Acknowledgments

CF was funded through NSF Award # 1908167. Authors acknowledge the NSF MRI: ECCS: 1726636 for XPS and MCF-AMPAC facility at the University of Central Florida. The authors

This is the author's peer reviewed, accepted manuscript. However, the online version of record will be different from this version once it has been copyedited and typeset.
PLEASE CITE THIS ARTICLE AS DOI: 10.1116/6.0002018

(KAR, JS, AK, MC) acknowledge the financial support of AFOSR through grant # FA9550-19-1-0127. MC's work was partially supported by the University of Central Florida under the Pre-eminent Postdoctoral Program (P³).

VI. Author Declarations

A. Conflict of Interest

The authors have no conflicts to disclose.

VII. Data Availability

The data that support the findings of this study are available from the corresponding author upon reasonable request.

References

1. H. Morkoç, S. Strite, G. B. Gao, M. E. Lin, B. Sverdlov and M. Burns, *J. Appl. Phys.* **76**, 3, 1363-1398 (1994).
2. G. V. Astakhov, D. R. Yakovlev, V. P. Kochereshko, W. Ossau, W. Faschinger, J. Puls, F. Henneberger, S. A. Crooker, Q. McCulloch, D. Wolverson, N. A. Gippius and A. Waag, *Phys. Rev. B* **65**, 16 (2002).
3. E. Monroy, F. Omnès and F. Calle, *Semicond. Sci. Technol.* **18**, 4, R33 (2003).
4. R. M. Park, M. B. Troffer, C. M. Rouleau, J. M. Depuydt and M. A. Haase, *Appl. Phys. Lett.* **57**, 20, 2127-2129 (1990).
5. I. Yonenaga, *Physica B Condens. Matter.* **308-310**, 1150-1152 (2001).
6. I. Yonenaga, K. Watanabe, S. Itoh and S. Fujiwara, *J. Mater. Sci.* **41**, 9, 2601-2604 (2006).
7. C. Walker, J. DePuydt, M. Haase, J. Qiu and H. Cheng, *Physica B Condens. Matter.* **185**, 1-4, 27-35 (1993).
8. A. Nurmikko, presented at the Extended abstract of the 1992 International Conference on Solid State Devices and Materials, 1992 (unpublished).
9. M. Godlewski, M. Skrobot, E. Guziewicz and M. R. Phillips, *J. Lumin.* **125**, 1, 85-91 (2007).
10. L. A. Kolodziejski, R. L. Gunshor and A. V. Nurmikko, *Annu. Rev. Mater. Sci.* **25**, 1, 711-755 (1995).
11. H. Jeon, J. Ding, W. Patterson, A. V. Nurmikko, W. Xie, D. C. Grillo, M. Kobayashi and R. L. Gunshor, *Appl. Phys. Lett.* **59**, 27, 3619-3621 (1991).

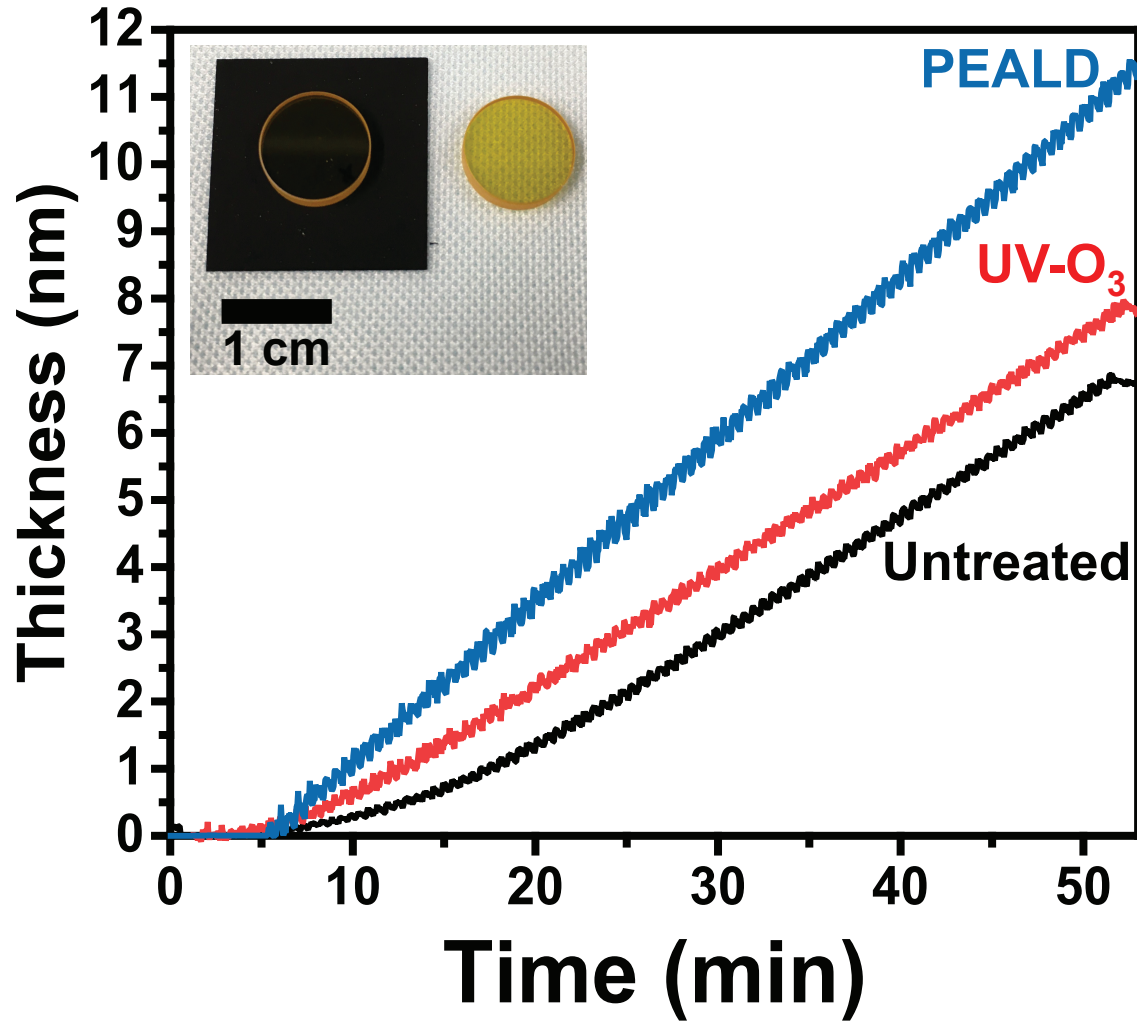
12. S. B. Mirov, V. V. Fedorov, D. Martyshkin, I. S. Moskalev, M. Mirov and S. Vasilyev, *IEEE J. Sel. Top Quantum Electron.* **21**, 1, 292-310 (2015).
13. M. Chazot, C. Arias, M. Kang, C. Blanco, A. Kostogiannes, J. Cook, A. Yadav, V. Rodriguez, F. Adamietz, D. Verreault, S. Danto, T. Loretz, A. Seddon, D. Furniss, K. Schepler, M. C. Richardson and K. A. Richardson, *J. Non-Cryst. Solids* **555**, 120619 (2021).
14. A. Yang, J. Qiu, J. Ren, R. Wang, H. Guo, Y. Wang, H. Ren, J. Zhang and Z. Yang, *J. Non-Cryst. Solids* **508**, 21-25 (2019).
15. E. V. Karaksina, L. A. Ketkova, M. F. Churbanov and E. M. Dianov, *Inorg. Mater.* **49**, 3, 223-229 (2013).
16. R. A. Mironov, E. V. Karaksina, A. O. Zabezhailov, R. M. Shapashnikov, M. F. Churbanov and E. M. Dianov, *Quantum Electron.* **40**, 9, 828-829 (2010).
17. D. Martyshkin, J. Goldstein, V. Fedorov and S. Mirov, *Opt. Lett.* **36**, 9, 1530-1532 (2011).
18. E. V. Karaksina, V. S. Shiryaev and L. A. Ketkova, *J. Non-Cryst. Solids* **377**, 220-224 (2013).
19. J. Cook, M. Chazot, A. Kostogiannes, R. Sharma, C. Feit, J. Sosa, P. Banerjee, M. Richardson, K. A. Richardson and K. L. Schepler, *Opt. Mater. Express* **12**, 4, 1555 (2022).
20. V. R. Rai, V. Vandalon and S. Agarwal, *Langmuir* **28**, 1, 350-357 (2012).
21. M. Chazot, A. Kostogiannes, M. Julian, C. Feit, J. Sosa, M. Kang, C. Blanco, J. Cook, V. Rodriguez and F. Adamietz, *J. Non-Cryst. Solids*, 121259 (2021).
22. L. A. Giannuzzi and F. A. Stevie, *Micron* **30**, 3, 197-204 (1999).
23. L. A. Giannuzzi, J. L. Drown, S. R. Brown, R. B. Irwin and F. A. Stevie, *Microsc. Res. Tech.* **41**, 4, 285-290 (1998).

24. M. Schaffer, B. Schaffer and Q. Ramasse, *Ultramicroscopy* **114**, 62-71 (2012).
25. B. Kempshall, L. Giannuzzi, B. Prenitzer, F. Stevie and S. Da, *J. Vac. Sci. Technol.*, B **20**, 1, 286-290 (2002).
26. J. L. Van Hemmen, S. B. S. Heil, J. H. Klootwijk, F. Roozeboom, C. J. Hodson, M. C. M. Van De Sanden and W. M. M. Kessels, *J. Electrochem. Soc.* **154**, 7, G165 (2007).
27. V. Mittal, N. P. Sessions, J. S. Wilkinson and G. S. Murugan, *Opt. Mater. Express* **7**, 3, 712-725 (2017).
28. J. R. Shallenberger and N. Hellgren, *Surf. Sci. Spectra* **27**, 1, 014020 (2020).
29. N. Hellgren, M. A. Steves, J. Shallenberger, S. K. O'Boyle, E. Mellott and A. R. Noble, *Appl. Surf. Sci.* **528**, 146604 (2020).
30. J. F. Moulder, W. F. Stickle, P. E. Sobol and K. D. Bomben, *Phys. Electron*, 230-232 (1995).
31. A. M. Chaparro, C. Maffiotte, M. T. Gutiérrez and J. Herrero, *Thin Solid Films* **358**, 1-2, 22-29 (2000).
32. J. D. McCullough, *J. Am. Chem. Soc.* **59**, 5, 789-794 (1937).
33. H. Nohira, W. Tsai, W. Besling, E. Young, J. Pétry, T. Conard, W. Vandervorst, S. De Gendt, M. Heyns and J. Maes, *J. Non-Cryst. Solids* **303**, 1, 83-87 (2002).
34. I. Iatsunskyi, M. Kempński, M. Jancelewicz, K. Załęski, S. Jurga and V. Smyntyna, *Vacuum* **113**, 52-58 (2015).
35. W. Chen, A. Kahn, P. Soukiassian, P. Mangat, J. Gaines, C. Ponzoni and D. Olego, *Phys. Rev. B* **51**, 20, 14265 (1995).
36. A. Olin, G. Nolang, E. Osadchii, L. Ohman, E. Rosen and Elsevier Sci. (2005).

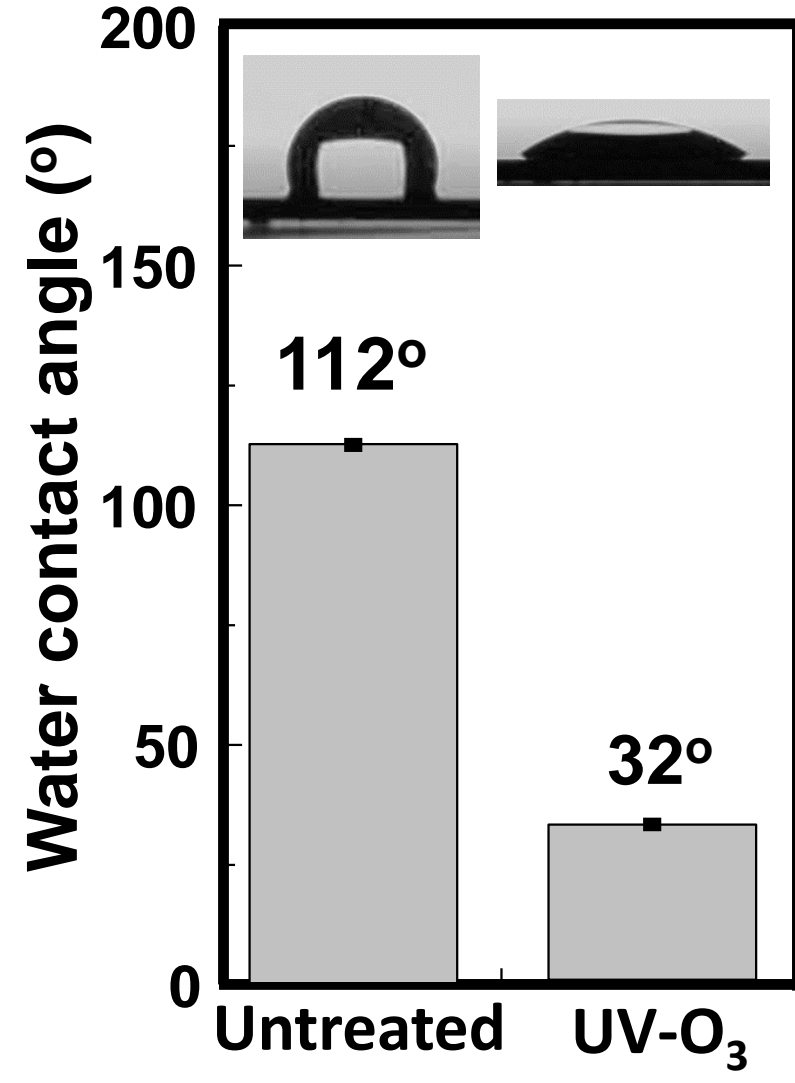
This is the author's peer reviewed, accepted manuscript. However, the online version of record will be different from this version once it has been copyedited and typeset.
PLEASE CITE THIS ARTICLE AS DOI: 10.1116/6.0002018

37. A. Chaparro, C. Maffiotte, J. Herrero and M. Gutiérrez, Surf. Interface Anal. **30**, 1, 522-526 (2000).
38. R. F. Brebrick, J. Phase Equilibria **21**, 3, 235-240 (2000).
39. O. Kubaschewski, Int. Ser. Mater. Sci. Technol. **24**, 478 (1977).

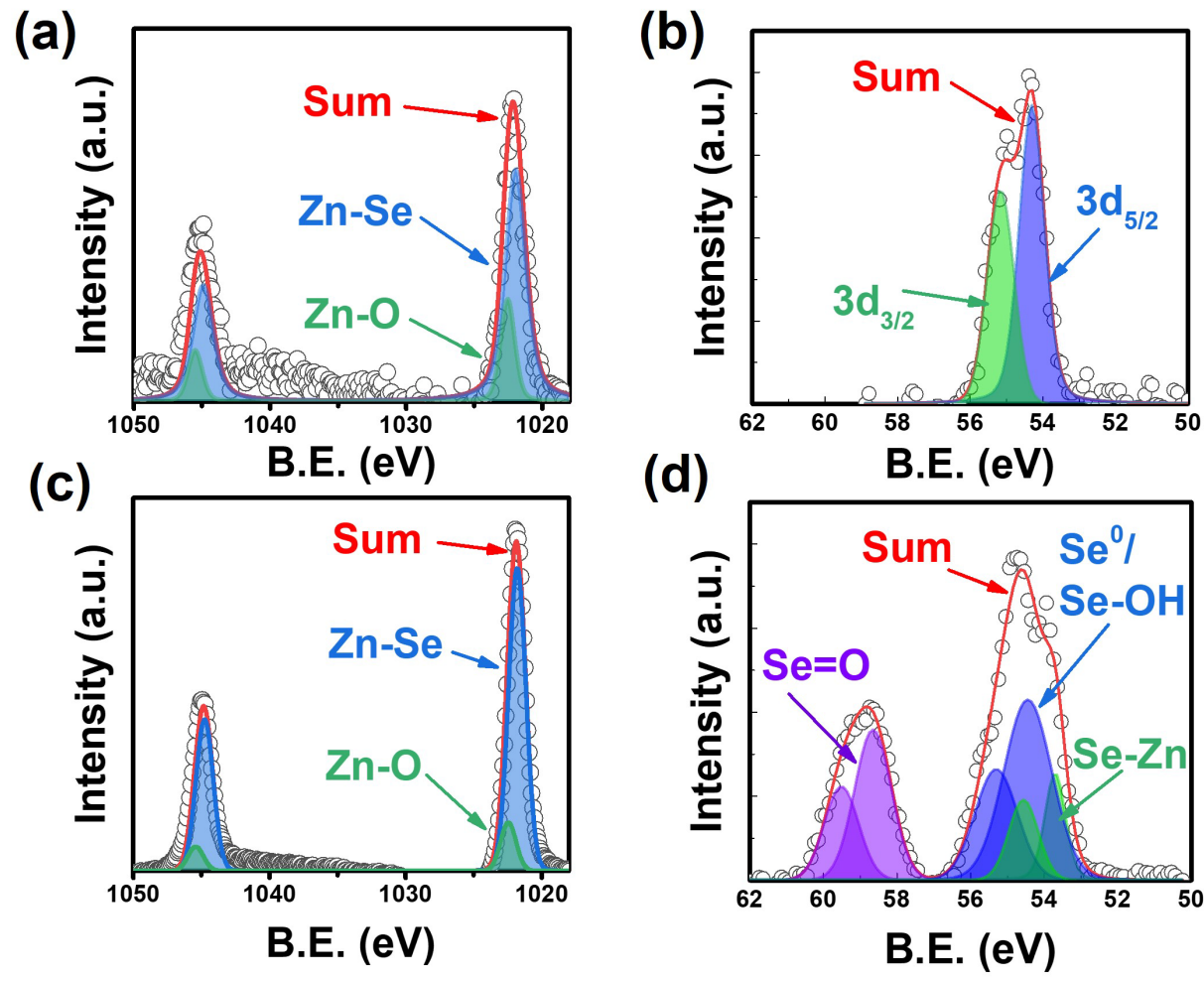
This is the author's peer reviewed, accepted manuscript. However, the online version of record will be different from this version once it has been copyedited and typeset.
PLEASE CITE THIS ARTICLE AS DOI: 10.1116/1.50002018



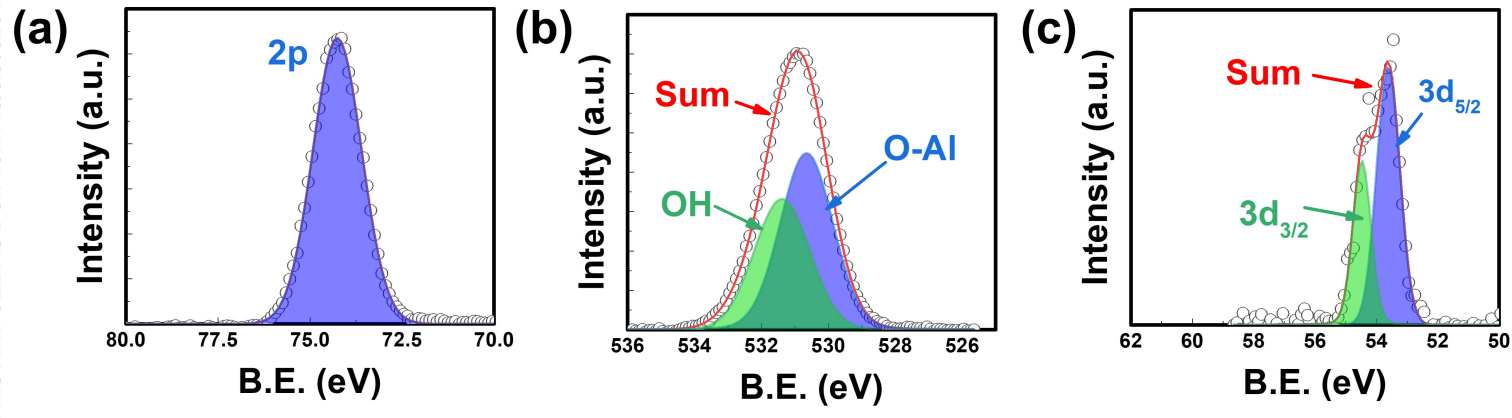
This is the author's peer reviewed, accepted manuscript. However, the online version of record will be different from this version once it has been copyedited and typeset.
PLEASE CITE THIS ARTICLE AS DOI: 10.1116/6.0002018



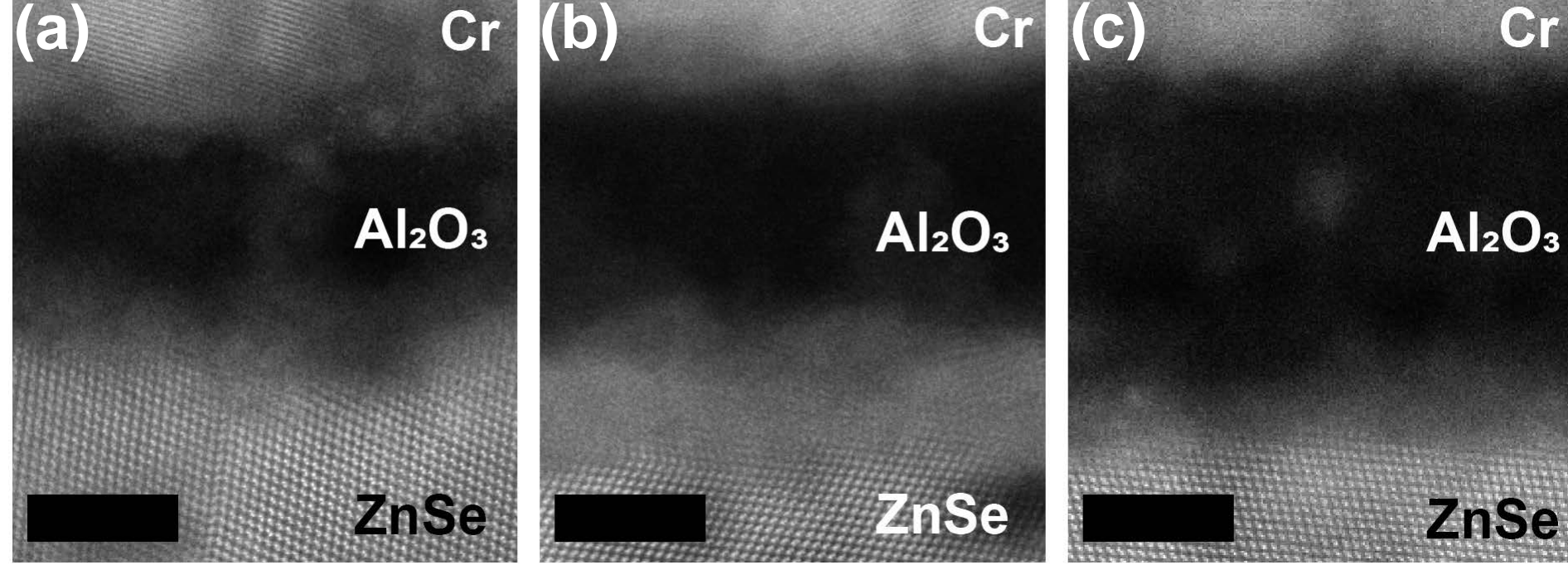
This is the author's peer reviewed, accepted manuscript. However, the online version of record will be different from this version once it has been copyedited and typeset.
PLEASE CITE THIS ARTICLE AS DOI: 10.1116/6.0002018



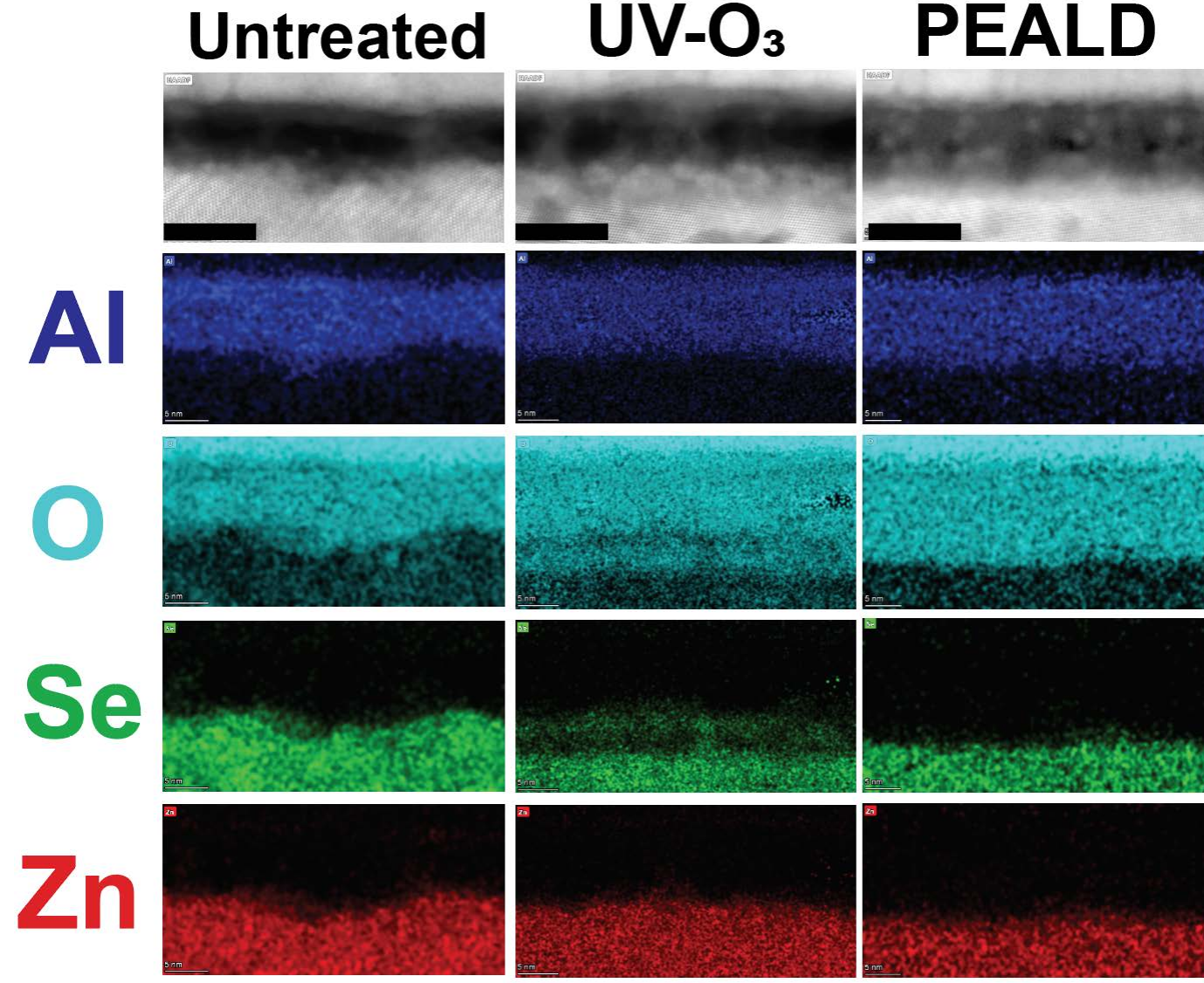
This is the author's peer reviewed, accepted manuscript. However, the online version of record will be different from this version once it has been copyedited and typeset.
PLEASE CITE THIS ARTICLE AS DOI: 10.1116/6.0002018



This is the author's peer reviewed, accepted manuscript. However, the online version of record will be different from this version once it has been copyedited and typeset.
PLEASE CITE THIS ARTICLE AS DOI: 10.1116/6.0002018



This is the author's peer reviewed, accepted manuscript. However, the online version of record will be different from this version once it has been copyedited and typeset.
PLEASE CITE THIS ARTICLE AS DOI: 10.1116/6.0002018



This is the author's peer reviewed, accepted manuscript. However, the online version of record will be different from this version once it has been copyedited and typeset.
PLEASE CITE THIS ARTICLE AS DOI: 10.1116/1.5002018

